Synthesis, Characterization and Electron Beam Assisted Decomposition of $(NO_2)[Au(NO_3)_4]$

Mathias S. Wickleder,*,† Oliver Büchner,† Frauke Gerlach,† Mandus Necke,† Katharina Al-Shamery,† Thomas Wich,‡ and Tim Luttermann‡

Institut für Reine and Angewandte Chemie and Division Microrobotics and Control Engineering, Universität Oldenburg, 26111 Oldenburg, Germany

Received January 8, 2008. Revised Manuscript Received April 19, 2008

Yellow single crystals of $(NO_2)[Au(NO_3)_4]$ (monoclinic, $P2_1/n$, $Z = 2$, $a = 775.1(2)$ pm, $b = 810.2(2)$ pm, $c = 898.7(2)$ pm, $\beta = 112.67(3)°$, $wR2 = 0.0622$) were obtained from the reaction of elemental gold with N_2O_5. In the crystal structure complex $[Au(NO_3)_4]^-$ ions are present with the Au^{3+} ions being in square planar coordination of four oxygen atoms of just as many monodentate nitrate groups. Charge compensation is achieved by linear NO_2^+ ions. $(NO_2)[Au(NO_3)_4]$ decomposes between 363 and 423 K in a complex process yielding elemental gold. Solutions of $(NO_2)[Au(NO_3)_4]$ in N_2O_5 were used to build contamination free structures of elemental gold onto a silica surface by electron beam initiated decomposition of the compound.

Introduction

The structuring of elemental gold is of great importance in various fields of application. One area of interest is lithographic processes for the production of optical and electrical devices, and typical procedures to build the desired gold structures include CVD techniques with the deposition initiated by a laser or an electron beam.[1–5] The drawback of CVD techniques is that usually organometallic compounds are used leading to a remarkable carbon contamination of the deposited gold.[6–8] Another important area where the structuring of elemental gold is mandatory is heterogeneous catalysis. In fact, the observation that elemental gold may act as catalyst has led to a remarkable renaissance of gold chemistry.[9–13] The catalytic activity is achieved when nanoparticles of gold are placed on certain substrates, most often oxides. The nanoparticles are produced by wet routes starting from $H[AuCl_4]$, usually followed by a calcination step.[14] These two examples may illustrate that there is a strong need for new precursor materials that can be used to produce elemental gold in defined structures. These precursors should contain no carbon to guarantee contamination free products. They should decompose at low temperature or under irradiation with a laser or an electron beam, and only gaseous decomposition products (beside the elemental gold) should be left behind. On our search for new gold precursors fulfilling these requirements we have investigated the ternary gold nitrates $M[Au(NO_3)_4]$ ($M = K-Cs, NH_4$)[15] of which the potassium compound has been described before[16] and the acidic species $(H_5O_2)[Au(NO_3)_4]\cdot H_2O$.[17] Following this route, we here present the preparation and the structural characterization of the gold nitrate $(NO_2)[Au(NO_3)_4]$ and a study of its thermal decomposition. The compound was prepared by the reaction of elemental gold and N_2O_5. The application of nitrogen oxides for the preparation of anhydrous nitrates was reported by Addison et al. in the early 1970s.[18] As products the authors often observed complex nitrates containing NO_2^+ or NO^+ ions. However, the products were usually characterized only by means of IR spectroscopy. We here present the reaction product of elemental gold with N_2O_5, the nitrylium compound $(NO_2)[Au(NO_3)_4]$, and its complete characterization. It will be shown that it is an excellent precursor for implementing gold structures on surfaces. The unique advantage of this nitrate compared to typical precursor compounds is that the

* To whom correspondence should be addressed. E-mail: mathias.wickleder@uni-oldenburg.de.
† Institut für Reine and Angewandte Chemie.
‡ Division Microrobotics and Control Engineering.

(1) Haight, J.; Aylett, M. R. In *Laser Microfabrication—Thin Film Processes and Lithography*; Ehrlich, D. J., Tsao, J. Y., Eds.; Academic Press: San Diego, 1989; p 453.
(2) Broers, A. N.; Molzen, W. W.; Cuomo, J. J.; Wittels, N. D. *Appl. Phys. Lett.* **1976**, *29*, 596.
(3) Hoffmann, P.; Utke, I.; Cicoira, F. Presented at 10th International Symposium "Nanostructures: Physics and Technology", St. Petersburg, Russia, 2002.
(4) Silvis-Cividijan, N. *Electron Beam Induced Nanometer Scale Deposition*; Delft University Press: Delft, The Netherlands, 2002.
(5) Folch, A.; Tejada, J.; Peters, C. H.; Wrighton, M. S. *Appl. Phys. Lett.* **1995**, *66*, 2080.
(6) Baum, T. H.; Jones, C. R. *Appl. Phys. Lett.* **1985**, *47*, 538.
(7) Baum, T. H.; Jones, C. R. *J. Vac. Sci. Technol.* **1986**, *4*, 1187.
(8) Baum, T. H.; Marinero, E. E.; Jones, C. R. *Appl. Phys. Lett.* **1986**, *49*, 1213.
(9) Ishida, T.; Haruta, M. *Angew. Chem.* **2007**, *119*, 7288.
(10) Hashmi, A. S. K.; Hutchings, G. J. *Angew. Chem.* **2006**, *118*, 8064.
(11) Bond, G. C.; Thompson, D. *Catal. Rev. Sci. Eng.* **1999**, *41*, 319.
(12) Haruta, M. *Catal. Surv. Jpn.* **1997**, *1*, 61.
(13) Kahlich, M. J.; Gasteiger, H. A.; Behm, R. J. *J. Catal.* **1999**, *182*, 430.
(14) Moreau, F.; Bond, G. C.; Taylor, A. O. *J. Catal.* **2005**, *231*, 105.
(15) Büchner, O. Ph.D. Thesis, Universität Oldenburg, Oldenburg, Germany, 2005.
(16) Garner, C. D.; Wallwork, S. C. *J. Chem. Soc. A* **1970**, 3092.
(17) Büchner, O.; Wickleder, M. S. *Z. Anorg. Allg. Chem.* **2004**, *630*, 1079.
(18) Addison, C. C.; Brownlee, G. S.; Logan, N. *J. Chem. Soc., Dalton Trans.* **1972**, 1440.
(19) Field, B. O.; Hardy, C. J. *J. Chem. Soc.* **1964**, 4428.

10.1021/cm800066r CCC: $40.75
Published on Web 07/29/2008

Table 1. $(NO_2)[Au(NO_3)_4]$: Crystallographic Data and Their Determination

lattice parameters	$a = 775.1(2)$ pm $b = 810.2(2)$ pm c = 898.7(2) pm $\beta = 112.67(3)°$
cell volume	520.8(2) Å^3
no. of formula units	2
crystal system	monoclinic
space group	$P2_1/n$ (No. 14)
measuring device	Stoe IPDS I
radiation	Mo Kα (graphite monochromator, $\lambda = 71.07$ pm)
temperature	20 °C
theta range	$5° < 2\theta < 54°$
index range	$-9 \le h \le 9$ $-10 \le k \le 10$ $-11 \le l \le 11$
rotation angle; φ increment	$0° < \varphi < 200°$; 2°
no. of exposures	100
exposure time	10 min
detector distance	60 mm
data corrections	Polarization and Lorentz factors
absorption correction	numerical
μ	14.23 mm^{-1}
measured reflections	4416
unique reflections	1137
with $I_0 > 2\sigma(I)$	617
no. of variables	95
R_{int}	0.1224
structure determinations	SHELXS-86 and SHELXL-93
scattering factors	intern.
extinction coefficient	0.0010(4)
goodness of fit (obs/all)	0.805/0.805
$R1$; $wR2$ ($I_0 > 2\sigma(I)$)	0.0337; 0.0534
$R1$; $wR2$ (all data)	0.0985; 0.0622
min./max. electron density, e Å^{-3}	−1.640/1.127
depository number	414094

gold structures obtained are completely free of highly undesired contaminations like carbon or chlorine.

Experimental Section

Synthesis. $(NO_2)[Au(NO_3)_4]$ was obtained from the oxidation of elemental gold with N_2O_5. The latter was prepared by the reaction of fuming HNO_3 with P_2O_5 as described in ref 18 and directly condensed on small pieces of elemental gold in a Schlenk tube. Upon gentle heating on a water bath (40 °C) the gold dissolves slowly in the liquid N_2O_5 yielding a yellow solution. The observation of a brown colored gas during the reaction indicates the formation of NO_2. After two days the solution was evaporated leading to a yellow powder of $(NO_2)[Au(NO_3)_4]$. If the evaporation was carried out slowly, even small yellow single crystals grow on the walls of the tube. $(NO_2)[Au(NO_3)_4]$ is very hygroscopic and turns immediately brown when exposed to air, probably due to the formation of $Au(OH)_3$.

X-ray Crystallography. Several crystals were selected in a glovebox and sealed in glass capillaries. They showed a monoclinic unit cell, and for the respective best specimen, diffraction data were collected using an image plate diffractometer (IPDS I, STOE & CIE). The structure solution was successful with direct methods provided by the program SHELXS-86[20] assuming the space group $P2_1/n$.[29] The subsequent full matrix least-squares refinement with SHELXL-93[21] led to the data summarized in the Tables 1–3. A

Table 2. $(NO_2)[Au(NO_3)_4]$: Atomic Positions and Equivalent Thermal Displacement Parameters[a]

atom	Wyckoff	*x/a*	*y/b*	*z/c*	$U_{eq} \times 10^{-1}$, pm^2
Au1	2*a*	0	0	0	23.2(2)
N3	2*b*	0	0	1/2	29(3)
N2	4*e*	0.365(1)	0.073(2)	0.225(1)	36(2)
O11	4*e*	0.681(1)	0.808(1)	0.252(1)	44(2)
O21	4*e*	0.005(1)	0.343(1)	0.778(1)	55(3)
O22	4*e*	0.2462(9)	0.114(1)	0.0747(8)	31(2)
O23	4*e*	0.321(1)	0.957(1)	0.293(1)	36(3)
N1	4*e*	0.168(1)	0.766(1)	0.864(1)	31(2)
O13	4*e*	0.248(1)	0.734(1)	0.005(1)	44(2)
O12	4*e*	0.049(1)	0.896(1)	0.8177(8)	34(2)
O31	4*e*	0.102(1)	0.910(1)	0.488(1)	43(2)

[a] Note: $U_{eq} = 1/3[U_{22} + 1/(\sin^2\beta)(U_{11} + U_{33} + 2U_{13}\cos\beta)]$.

Table 3. Selected Distances (pm) and Angles (deg) for $(NO_2)[Au(NO_3)_4]$

Au−O12	2×	200.7(8)	O12−Au−O12		180
Au−O22	2×	199.0(7)	O22−Au−O22		180
			O12−Au−O22	2×	90.7(3)
			O22−Au−O12	2×	89.3(3)
N1−O11		121(1)	O11−N1−O12		113.3(9)
N1−O12		135(1)	O11−N1−O13		126.(1)
N1−O13		120(1)	O12−N1−O13		120.8(9)
N2−O21		121(1)	O21−N2−O22		114.7(11)
N2−O22		135(1)	O21−N2−O23		127.2(11)
N2−O23		124(1)	O22−N2−O23		118.1(10)
N3−O31	2×	111.2(9)	O31−N3−O31		180

numerical absorption correction was applied to the data with the help of the programs X-RED and X-SHAPE.[22,23]

Thermal Analysis. DTA/TG measurements were performed with the help of a thermal analyzer (TGA/SDTA 851^E, METTLER-TOLEDO). For that purpose about 10 mg of the substance was filled in a corundum container and heated with a constant rate of 10 K/min under flowing argon. The thermal decomposition was followed from 303 K up to 773 K. Characteristic points like onset and end temperatures of the thermal effects were taken from the differentiated DTA curve following common procedures using the software delivered with the analyzer.[24] An electron microscopic as well as an energy dispersive X-ray analysis (EDAX) investigation of the thermally decomposed material was performed with the microscope XL 40 (Philips, NL).

Electron Beam Assisted Decomposition. Electron beam assisted decomposition was carried out by irradiating a precursor coated silicon wafer with the focused electron beam of a FEI Quanta 600 scanning electron microscope (SEM). The wafer was coated by dropping a solution of $(NO_2)[Au(NO_3)_4]$ in N_2O_5 on the wafer surface. Then the wafer was transferred from the glovebox under nitrogen atmosphere to the vacuum chamber of the SEM. After pumping down to a pressure of 10^{-5} mbar, the precursor coated wafer was irradiated with the electron beam by point, line, and area scans of dose densities between 10 and 1000 C·m^{-2}. After structuring with the electron beam, the sample was taken out of the vacuum chamber and the unexposed precursor was rinsed away with water. The developed structures were examined with the same SEM and by means of qualitative EDAX analysis.

X-ray Photoelectron Spectroscopy (XPS). An as prepared precursor-coated silicon wafer was also investigated in an ultrahigh vacuum chamber (base pressure of 3×10^{-10} hPa) equipped with XPS and QMS. The sample was irradiated by Mg $K\alpha_{1,2}$ photons

(20) Sheldrick, G. M. *SHELXS86, Programme zur Röntgenstrukturanalyse*; Universität Göttingen: Göttingen, Germany, 1986.
(21) Sheldrick, G. M. *SHELXL93, Program for the Refinement of Crystal Structures*; Universität Göttingen: Göttingen, Germany, 1993.
(22) *X-RED 1.07, Data Reduction for STADI4 and IPDS*; Stoe & Cie: Darmstadt, Germany, 1996.
(23) *X-SHAPE 1.01, Crystal Optimisation for Numerical Absorption Correction*; Stoe & Cie: Darmstadt, Germany, 1996.
(24) *STAR^e, Thermal analysis for the analyzer TGA/SDTA 851^E*, version 8.1; Mettler-Toledo GmbH: Schwerzenbach, Germany, 2004.

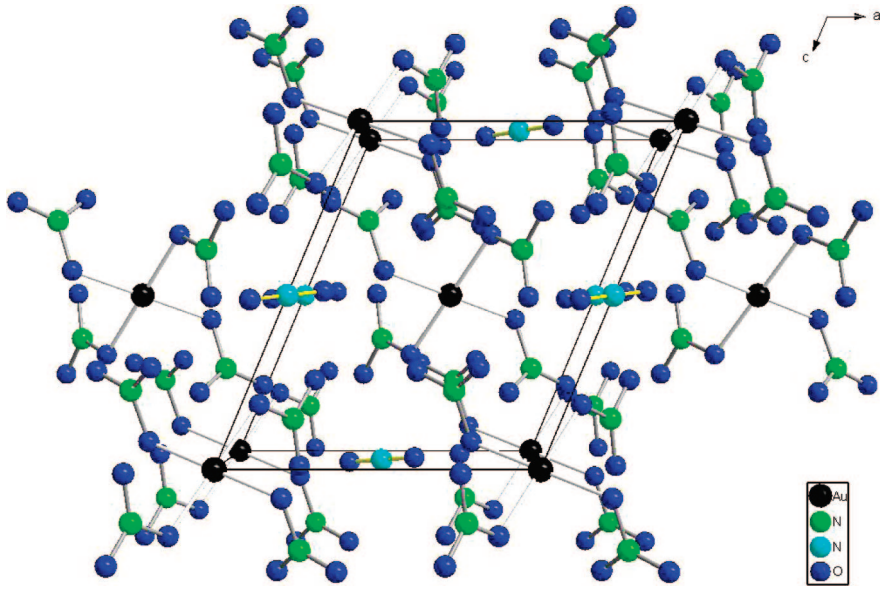

Figure 1. Perspective view of the crystal structure of $(NO_2)[Au(NO_3)_4]$ along [010]. The nitrogen atoms of the NO_2^+ ions are drawn in turquoise color.

(kinetic energy 1253.6 eV) generated by a SPECS XR-50 X-ray gun. The emitted electrons were analyzed by a hemispheric energy analyzer (Leybold EA-10) and detected with an electron multiplier system (Leybold).

The X-ray photoelectron spectra were taken at room temperature. The precursor decomposition was done by heating the silicone wafer to 620 K through thermal radiation by a filament from the back. Debuting gases were characterized by a quadrupole mass spectrometer (Pfeiffer QMS/QMA-200).

Results and Discussion

Crystal Structure. $(NO_2)[Au(NO_3)_4]$ crystallizes monoclinically with space group $P2_1/n$ and contains complex $[Au(NO_3)_4]^-$ anions and linear NO_2^+ ions (Figure 1). The gold atom of the complex anion is situated on a special site of space group $P2_1/n$ (0, 0, 0, Wyckoff position 2*a*) and coordinated by four monodentate nitrate ions which belong to two different crystallographic species, $N(1)O_3^-$ and $N(2)O_3^-$. The distances Au−O are 199.7 (2×) and 200.7 (2×) pm, and the angles O−Au−O differ only slightly from 90° and 180° so that the coordination of Au^{3+} is nearly ideal square-planar (Table 3). Within the nitrate ions the distances N−O are significantly longer for those oxygen atoms that are bonded to Au^{3+} ions (Table 3). The same observations were made for the tetranitratoaurates known so far.[15–17] The charge balance for the $[Au(NO_3)_4]^-$ ions is achieved by nitrylium ions, NO_2^+ (Figure 2). Within the linear ions, two crystallographically equivalent oxygen atoms are bonded to the central nitrogen atom at a distance of 111.2 pm. This value matches quite well the findings for other nitrylium compounds.[25,26]

The nitrogen atom of the NO_2^+ ion is located on the site 2*b* (0, 0, 1/2) of the space group $P2_1/n$. Interestingly, this is exactly the position of the K^+ ion in $K[Au(NO_3)_4]$. Both crystal structures exhibit the same space group, but due to the different coordination requirements of K^+ and NO_2^+ ions, respectively, the lattice constants of both nitrates differ remarkably ($K[Au(NO_3)_4]$: $a = 837.1$, $b = 705.9$, $c = 917.2$ pm, $\beta = 111.14°$; $(NO_2)[Au(NO_3)_4]$: $a = 775.1$, $b = 810.2$, $c = 898.7(2)$ pm, $\beta = 112.67(3)°$). While the K^+ ion is in 10-fold coordination of oxygen atoms, the NO_2^+ ions in $(NO_2)[Au(NO_3)_4]$ have eight oxygen neighbors with a distance between 273 and 330 pm to the central nitrogen atom, and further contacts occur only above 365 pm. Furthermore, the nonspherical shape of the NO_2^+ ions and their orientation in the [010] direction causes a remarkable lengthening of the *b* axis compared to the potassium compound.

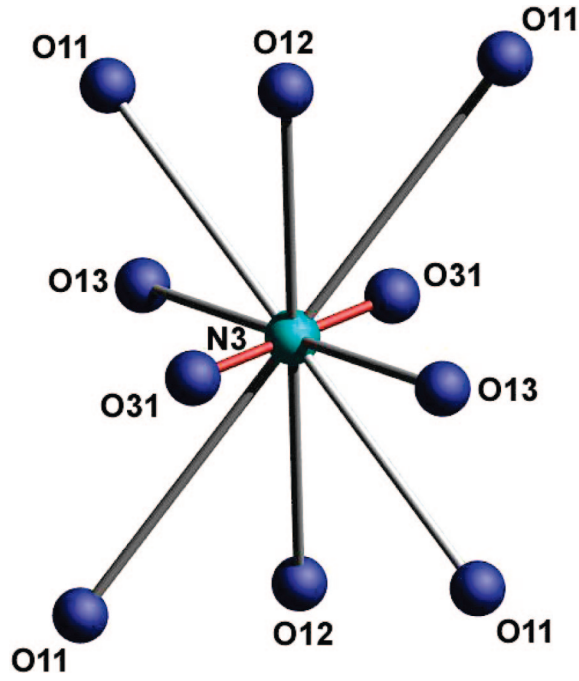

Figure 2. Coordination of the linear NO_2^+ ions in the crystal structure of $(NO_2)[Au(NO_3)_4]$. The two bonds within the cation are drawn in red. The distances of the central nitrogen atom to further oxygen atoms range from 273 to 330 pm.

(25) Tikhomirov, G.; Morozow, I.; Znamenkov, K.; Kemnitz, E.; Troyanov, S. *Z. Anorg. Allg. Chem.* **2002**, *628*, 872.
(26) Colombo, D. G.; Young, V. G.; Gladfelter, W. L. *Inorg. Chem.* **2000**, *39*, 4621.

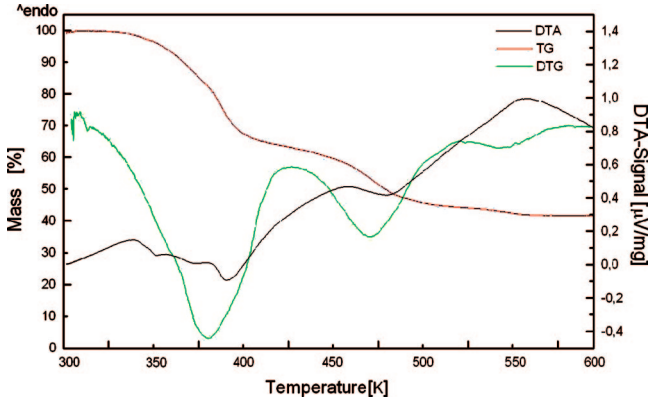

Figure 3. DTA/TG diagram of the thermal decomposition of (NO_2)-$[Au(NO_3)_4]$.

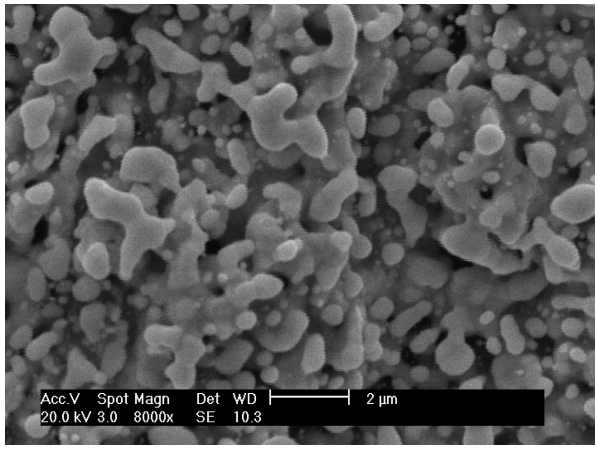

Figure 4. Electron microscopic picture of the decomposition residue of $(NO_2)[Au(NO_3)_4]$.

Thermal Decomposition. The thermal decomposition of $(NO_2)[Au(NO_3)_4]$ is roughly a two step process, and with respect to the observed mass loss it leads to elemental gold (Figure 3). However, inspection of the DTG curve shows that probably further steps are involved. Unfortunately they are not well resolved and also other heating rates did not yield reasonable improvement. Thus a detailed interpretation is difficult. The onset of the first well resolved decomposition step is at 330 K and the reaction is complete at 440 K. The maximum of the peak is at 390 K. The TG curve shows a mass loss of about 39% corresponding to 192 mass units. The intermediate product has not been investigated so far. The onset of the second decomposition step is at 449 K and the decomposition is completed at 550 K. The maximum peak is at 482 K. The overall mass loss of 58% differs only slightly from the calculated mass loss of 60% for the formation of elemental gold as the decomposition product. The residue of the thermal decomposition of (NO_2)-$[Au(NO_3)_4]$ was investigated by electron microscopy and EDAX. The EDAX investigation identified the residue as pure gold. From the electron microscopic picture (Figure 4) we can conclude that the size of the gold particle is at about 500 nm and below. In our previous investigations of ternary gold nitrates the minimum for gold particle sizes was around 500−1000 nm.[15] Similar results were obtained in UHV experiments in which the products of decomposition can be measured in the gas phase with the aid of a quadrupole mass spectrometer as a function of surface temperature while the surface reaction itself can be followed by XPS.[27]

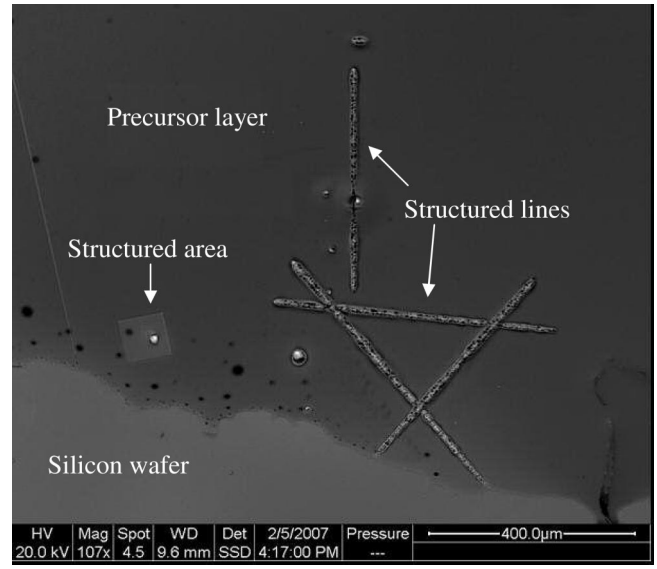

Figure 5. Electron beam initiated deposition of elemental gold on a silicon wafer. The wafer was coated with a solution of $(NO_2)[Au(NO_3)_4]$ in N_2O_5 and different structures (dots, lines, areas) were directly written into the precursor layer.

Electron Beam Assisted Decomposition. Irradiation of the precursor on the silicon substrate with dose densities between 10 and 1000 $C \cdot m^{-2}$ leads to decomposition of the precursor. The decomposed precursor material is recognizable in the SEM by its brighter appearance on the SE (secondary electrons) as well as BSE (backscatter electron) images (Figure 5). This indicates that the topography as well as the material composition changed through the irradiation. After development by rinsing with water, the developed structures were analyzed in the SEM and by qualitative EDAX analysis. The SEM images revealed that the unexposed precursor was washed away completely and only the exposed structures are left on the substrate surface. Qualitative EDAX analysis of the structures showed a very high gold signal and no oxygen and nitrogen signals, respectively.

X-ray Photoelectron Spectroscopy. The spectra for the Au 4f regime of the sample before and after decomposition are given in Figure 6. The dashed−dotted−dotted line in both spectra describes the Au 4f doublet signal composed by Au $4f_{5/2}$ (∼87.7 eV) and Au $4f_{7/2}$ (∼84.0 eV), which is characteristic for elemental gold. After decomposition only elemental gold can be found.

Before decomposition the spectrum is complex and two more Au 4f species (dashed line and dashed−dotted line) can be found at higher binding energies. The major Au 4f species (dashed line, 93.0 and 89.4 eV) is strongly shifted with respect to elemental gold and can be assumed as Au^{3+} of $(NO_2)[Au(NO_3)_4]$. (Strong shifts of Au^{3+} species (91.6 and 88.1 eV) can also be found for other gold precursors like $[Au(en)_2]Cl_3$.[30])

The secondary ionic Au 4f species (dashed−dotted line, 90.4 and 86.8 eV) are possibly $(NO_2)[Au(NO_3)_4]$ or impuri-

(27) Necke, M.; Gerlach, F.; Wickleder, M. S.; Klüner, Th.; Al-Shamery, K. In preparation.

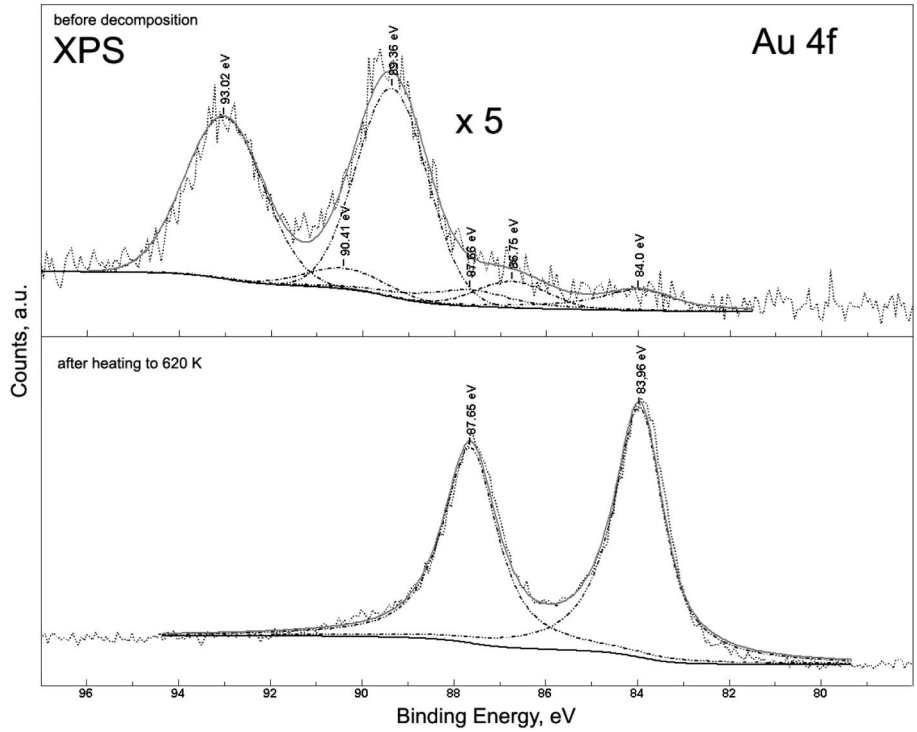

Figure 6. Au 4f X-ray signal of $(NO_2)[Au(NO_3)_4]$ on a silicon wafer after and before decomposition.

ties due to water. Similar peaks in Au_2O_3 (90.65 and 86.97 eV) are assigned to Au^{3+} hydroxyl species while oxidic Au^{3+} of Au_2O_3 is related to 88.70 and 85.05 eV.[31]

Conclusion

In this paper we have presented the new gold precursor $(NO_2)[Au(NO_3)_4]$ which was prepared by the reaction of elemental gold and N_2O_5. The crystal structure and the thermal behavior of the compound were investigated. Furthermore, solutions of $(NO_2)[Au(NO_3)_4]$ in N_2O_5 were successfully used for the structuring of gold on a silicon wafer by electron beam assisted decomposition.[28]

Acknowledgment. This work was supported by the Deutsche Forschungsgemeinschaft. O.B. acknowledges support by the Fonds der Chemischen Industrie for a doctoral stipend.

Supporting Information Available: Crystallographic data in CIF format. This material is available free of charge via the Internet at http://pubs.acs.org. Furthermore, the data have been deposited with the Fachinformationszentrum Karlsruhe, D-76344 Eggenstein-Leopoldshafen (crysdata@FIZ-Karlsruhe.de), and are available upon quoting the deposition number given in Table 1.

CM800066R

(28) Wich, Th.; Al-Shamery, K.; Luttermann, T.; Wickleder, M.; Gerlach, F.; Necke, M.; Schnars, H.; Büchner, O. Elektronengestütztes additives Strukturierungsverfahren zur direkten Abscheidung von Metallen. German Patent 102007018845.7-45, 2007.
(29) Hahn, Th., Ed. *International Tables for Crystallography*; D. Reidel Publishing Company: Dordrecht, 1983; Vol. C.
(30) Bulushev, D. A.; Yuranov, I.; Suvororva, E. I.; Buffat, P. A.; Kiwi-Minisker, L. *J. Catal.* **2004**, *224*, 8.
(31) Christ, V. B. *Handbook of Monochromatic XPS Spectra−Volume Two: Commercially Pure Binary Oxides*; XPS International LLC: Mountain View, CA, 2005.